

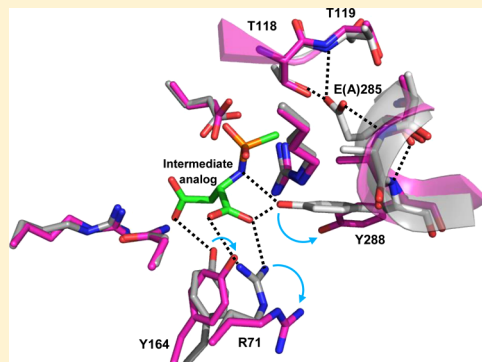
# Aspartoacylase Catalytic Deficiency as the Cause of Canavan Disease: A Structural Perspective

Yasanandana S. Wijayasinghe, Alexander G. Pavlovsky, and Ronald E. Viola\*

Department of Chemistry and Biochemistry, The University of Toledo, Toledo, Ohio 43606, United States

**S Supporting Information**

**ABSTRACT:** Canavan disease (CD) is a fatal, childhood neurological disorder caused by mutations in the *ASPA* gene, leading to catalytic deficiencies in the aspartoacylase (ASPA) enzyme and impaired *N*-acetyl-L-aspartic acid metabolism in the brain. To study the possible structural defects triggered by these mutations, four *ASPA* missense mutations associated with different disease severities have been structurally characterized. These mutant enzymes each have overall structures similar to that of the native *ASPA* enzyme, but with varying degrees of alterations that offer explanations for the respective loss of catalytic activity. The K213E mutant, a nonconservative mutant associated with a mild disease phenotype, has minimal structural differences compared to the native enzyme. In contrast, the loss of van der Waals contacts in the F295S mutant and the loss of hydrophobic and hydrogen bonding interactions in the Y231C mutant lead to a local collapse of the hydrophobic core structure in the carboxyl-terminal domain, contributing to a decrease in protein stability. The structure of the E285A mutant, the most common clinical mutant, reveals that the loss of hydrogen bonding interactions with the carboxylate side chain of Glu285 disturbs the active site architecture, leading to altered substrate binding and lower catalytic activity. Our improved understanding of the nature of these structural defects provides a basis for the development of treatment therapies for CD.



Canavan disease (CD) is an inherited, progressive neurodegenerative disorder that occurs as a consequence of a defect in a single metabolic enzyme in the brain.<sup>1</sup> The clinical manifestations of CD typically become apparent ~3 months after birth, including macrocephaly, hypotonia, poor head control, developmental delay, and motor, visual, and verbal retardation. The devastating impact on the developing brain usually leads to a premature death in childhood.<sup>2</sup> CD has been reported in many populations but is more prevalent in the Ashkenazi Jewish community.<sup>3</sup> Mutations in the *ASPA* gene that encodes aspartoacylase (ASPA, EC 3.5.1.15) lead to insufficient metabolism of *N*-acetyl-L-aspartic acid (NAA) in the brain.<sup>4,5</sup> NAA acts as the acetyl group carrier, which is synthesized in the neuronal mitochondria and then transported to the oligodendrocytes where myelin formation takes place. In the oligodendrocytes, NAA is hydrolyzed by ASPA to generate L-aspartate and acetate, the precursor for myelin lipid biosynthesis (Figure 1).<sup>6</sup> Deficiency in ASPA activity results in an inadequacy of acetate and elevation of the level of NAA in the central nervous system, leading to poor myelination of neurons and the spongy degeneration of the white matter in the developing brain of Canavan patients.<sup>7,8</sup>

The human *ASPA* gene consists of six exons and encodes a 313-amino acid protein with a two-domain architecture. The first 212 residues of the enzyme form the amino-terminal domain, which consists of a central six-stranded  $\beta$ -bundle surrounded by eight  $\alpha$ -helices. The carboxyl-terminal domain is composed mainly of  $\beta$ -sheet and coil structures that wrap around the amino-terminal domain.<sup>9</sup> The enzyme ASPA exists

as a homodimer with the active site in each subunit formed primarily by residues in the N-terminal domain.<sup>9</sup> More than 70 different mutations in the *ASPA* gene have been reported in the human gene mutation database (<http://www.hgmd.org>), and the majority of these are missense mutations located remotely from the catalytic site of the enzyme. The E285A mutation is the most common missense mutation among Ashkenazi Jews,<sup>3</sup> comprising nearly 85% of the CD patients in this population. This clinical mutant has <1% residual activity compared to that of the native enzyme.<sup>10,11</sup> The ASPA K213E, Y231C, and F295S mutants are found in mild or variable disease phenotypes<sup>12–14</sup> with relative residual activities of 15, 24, and 10%, respectively.<sup>10</sup> In contrast, the K213E mutant was previously reported to have nativelike enzyme activity, and this mutation is found to be associated with the G274R mutation as a homozygous double mutation that results in slower progression of the disease.<sup>12</sup> These alterations each occur in highly conserved regions of the aspartoacylase primary structure, but none of them result in the replacement of amino acids that are directly involved in the catalytic activity of ASPA.<sup>15,16</sup> However, both *in vivo* and *in vitro* studies have found that the *ASPA* pathological missense mutations have lower protein stability and decreased cellular availability compared to those of the native enzyme.<sup>10,17</sup>

Received: June 10, 2014

Revised: July 4, 2014

Published: July 8, 2014

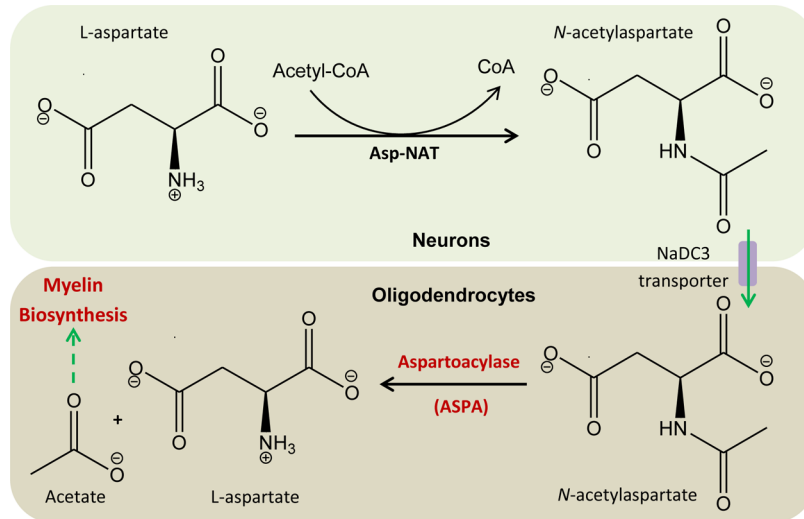


**Figure 1.** Schematic representation of the biological role of aspartoacylase (ASPA). ASPA catalyzes the deacetylation of N-acetyl-L-aspartate produced from L-aspartate and acetyl-CoA by the action of aspartate N-acetyltransferase (Asp-NAT) in the neurons. After being transported to the oligodendrocytes, the resulting acetate serves as the precursor for myelin lipid biosynthesis.

Because the loss of enzyme activity and stability appears to be dictated primarily by changes in protein structure, the three-dimensional structure of aspartoacylase mutants can provide molecular insights into Canavan disease and could guide the development of therapeutic approaches for the treatment of this devastating disease. No structural information has been available for any of the ASPA clinical mutations. Therefore, the effects of genetic mutations on the aspartoacylase structure are the focus of this study. Here we report and examine the first structures of four different aspartoacylase clinical mutants, including the predominant E285A mutation found in Jewish Canavan patients.

## EXPERIMENTAL PROCEDURES

**Protein Expression and Purification.** The human ASPA gene was cloned into the pPICZ A plasmid vector.<sup>18</sup> Each of the aspartoacylase clinical mutants was constructed by using the QuikChange II site-directed mutagenesis kit (Stratagene), the presence of the correct mutations being confirmed by DNA sequencing. Mutant enzymes were expressed in a *Pichia pastoris* (KM71H) yeast cell line and purified as described previously with only slight modifications.<sup>18</sup> The purity of the enzyme samples was determined by sodium dodecyl sulfate–polyacrylamide gel electrophoresis using 4 to 12% Bis-Tris precast gels (Life Technologies) and 2-(N-morpholino)ethanesulfonic acid (MES) running buffer. Aspartoacylase activity was measured by the previously reported aspartase-coupled enzyme assay.<sup>11</sup> The sample homogeneity and the oligomeric state of the clinical mutants were determined by light scattering using a DynaPro Titan DLS instrument (Wyatt Technology). Native polyacrylamide gel electrophoresis was performed using the dark blue cathode buffer and 3 to 12% Bis-Tris precast gels from Life Technologies. The concentration of the protein was measured at 280 nm by using a NanoDrop 2000 spectrophotometer (Thermo Fisher).

**Crystallization of Mutant ASPA.** Binary complex crystals of the aspartoacylase clinical mutants with a bound intermediate analogue were grown by the hanging-drop vapor diffusion method. The drop was formed with two parts of protein (4 mg/mL) solution incubated with 2 mM intermediate analogue

and one part of well solution containing 50 mM sodium citrate (pH 6.0), 300 mM K<sub>2</sub>HPO<sub>4</sub>, 3% ethylene glycol, 10 mM dithiothreitol, and 13–15% polyethylene glycol 3350. Needle-shaped crystals appeared at 277 K within 24 h but were not of sufficient quality for X-ray diffraction studies. After screening for additives (Hampton Research), we obtained improved rod-shaped crystals with 10–20 mM Na<sub>2</sub>EDTA at 277 K in 3–4 days. These crystals were transferred into a cryoprotecting solution containing 25% ethylene glycol in well solution and were then flash-frozen in liquid nitrogen for data collection. The ASPA intermediate analogue, N-phosphonomethyl-L-aspartate, was synthesized as reported previously.<sup>16</sup>

**Data Collection and Structure Determination.** X-ray diffraction data were collected at Advanced Photon Source beamline 23-ID-D at Argonne National Laboratory (Argonne, IL), using an image plate MARmosaic detector. Diffraction images were indexed and integrated with HKL2000<sup>19</sup> and scaled by Scalepack. The crystal structures were refined in REFMAC,<sup>20</sup> initially with rigid-body refinement followed by restrained refinement using the atomic coordinates of the human ASPA intermediate analogue binary complex from Protein Data Bank (PDB) entry 2O4H as the initial model.<sup>16</sup> Subsequent refinement was performed by iterative cycles of manual model building with COOT.<sup>21</sup> All figures were prepared with the PyMOL molecular graphics system, version 1.3.<sup>22</sup>

## RESULTS AND DISCUSSION

**Aspartoacylase Structure Refinement.** The aspartoacylase clinical mutants, K213E, Y231C, F295S, and E285A, have each been produced, purified, and cocrystallized with the intermediate analogue N-phosphonomethyl-L-aspartate by using polyethylene glycol 3350 as the precipitant. All four mutant enzyme forms crystallized as binary complexes in the same space group as the previously reported binary complex of the ASPA native enzyme,<sup>16</sup> and each of these crystal forms was found to diffract to medium resolution (Table 1). The structures of these mutants were refined for residues 10–310 in each subunit of the enzyme by using the intermediate analogue–native ASPA binary complex structure (PDB entry 2O4H) as the starting model. There was no interpretable electron density for the first nine residues at the

Table 1. X-ray Data Collection and Refinement Statistics

	K213E ASPA	Y231C ASPA	E285A ASPA	F295S ASPA
<b>Data Collection<sup>a</sup></b>				
wavelength (Å)	0.979	1.283	0.979	0.979
space group	P4 <sub>2</sub> 1 <sub>2</sub>			
unit cell dimensions				
$a = b, c$ (Å)	146.07, 103.42	147.96, 103.46	147.74, 102.74	146.17, 103.13
$\alpha = \beta = \gamma$ (deg)	90	90	90	90
resolution (Å)	46.25–2.60 (2.67–2.60)	48.88–2.90 (3.00–2.90)	46.76–3.00 (3.11–3.00)	46.27–2.80 (2.87–2.80)
no. of reflections	102690	123336	44136	84572
no. of unique reflections	28127	25970	17284	23349
completeness (%)	80.1 (30.8)	100.0 (99.9)	73.8 (16.3)	83.3 (40.2)
redundancy	3.7 (1.5)	4.7 (4.6)	2.6 (1.3)	3.6 (1.6)
$R_{\text{merge}}$ (%)	10.6 (20.6)	14.2 (74.4)	10.1 (18.8)	10.7 (25.1)
$I/\sigma_I$	10.5 (2.1)	10.7 (2.1)	9.4 (3.0)	10.8 (2.4)
<b>Refinement</b>				
no. of reflections, work/free	26625/1409	24598/1320	16360/886	22135/1191
$R_{\text{work}}/R_{\text{free}}$ (%)	19.9/23.4	19.7/23.5	19.3/24.0	18.4/23.7
root-mean-square deviation for bonds (Å)	0.007	0.008	0.007	0.010
root-mean-square deviation for angles (deg)	1.14	1.30	1.15	1.39
ESU from $R_{\text{free}}$ (Å)	0.287	0.309	0.445	0.340
no. of protein molecules	2	2	2	2
no. of atoms in the protein molecules	4842	4830	4834	4853
no. of atoms				
metal	2	2	2	2
ligand	26	26	26	26
water	67	24	33	72
average $B$ factor (Å <sup>2</sup> )	53.4	70.0	72.2	41.0
Ramachandran plot (%)				
favored regions	93.8	93.8	93.7	94.0
allowed regions	5.2	5.4	5.4	5.3
generously allowed regions	1.0	0.8	0.9	0.7
PDB entry	4mxu	4tnu	4nfr	4mri

<sup>a</sup>Statistics for the highest-resolution shell are given in parentheses.

amino terminus, as well as for the last three residues at the carboxyl terminus of the enzyme. In the case of Y231C and E285A ASPA, the final structures were obtained by applying local noncrystallographic symmetry-restrained refinement. The structures of all four mutants have crystallographic  $R$  factors of <20%, and the average difference between  $R_{\text{work}}$  and  $R_{\text{free}}$  is <5% (Table 1). The presence of the correct mutation in each structure was confirmed in the 2mF<sub>o</sub>–DF<sub>c</sub> difference maps (Figure 2).

**Comparison of the Mutant Aspartoacylase Oligomeric States.** Because native aspartoacylase is a functional dimer and some of the clinical mutations are located close to the dimer interface (Figure 3A), the effect of each mutation on subunit dimerization was evaluated to determine whether the observed loss of catalytic activity was a consequence of changes in the quaternary structure of the enzyme. Recombinant human ASPA was genetically engineered with a carboxyl-terminal hexahistidine tag, with a resulting calculated molecular mass of 36.4 kDa. Dynamic light scattering of ASPA clinical mutants K213E, Y231C, E285A, and F295S indicated the presence of a dimer in solution for each enzyme form, with a hydrodynamic radius of approximately 3.8 nm and a calculated molecular mass ranging from 73 to 78 kDa (Figure S1A of the Supporting Information). Native gel electrophoresis of ASPA also confirmed the dimeric states of these mutants in solution, and the dimer of ASPA E285A is stable in a solution with the addition of as much as 2 M urea (Figure S1B of the Supporting Information). These

mutants were also found to crystallize as homodimers, which is similar to what was observed for the native enzyme.

**Structural Roles of the Mutation Sites in Aspartoacylase.** Missense mutations at positions Lys213, Tyr231, Phe295, and Glu285 of ASPA have been reported in Canavan patients,<sup>3,12–14</sup> but these amino acid residues are not directly involved in catalysis.<sup>16</sup> Lys213 is a surface residue found distal to the active site (Figure 3A) and does not have any identifiable contacts within the protein structure. This positively charged lysine likely interacts with water molecules and helps to solvate the enzyme in its aqueous environment.

A nonsense mutation at the Tyr231 position is one of the founder mutations present in Ashkenazim.<sup>3</sup> Tyr231 is located in a loop structure in the carboxyl-terminal domain of aspartoacylase and is in apparent hydrogen bond contact with the hydroxyl group of Tyr289 and the side chain carbonyl oxygen of Asn284. These residues are located in a hydrophobic region surrounded by Ile239, Ile243, Phe262, Tyr289, and Ala294, as well as Leu187 from the adjacent subunit (Figure 4). The enzyme active site is found adjacent to this area, and substrate binding residue Tyr288 is in the same helix as Tyr289. Phe295 is found in a hydrophobic core at the carboxyl-terminal domain of ASPA (Figure 3A), and van der Waals interactions of Phe295 with the neighboring Val229, Ile243, Leu247, and Pro280 residues, along with the hydrocarbon chain of Lys297 (Figure 5), help to stabilize the structure of the enzyme. Replacement of this

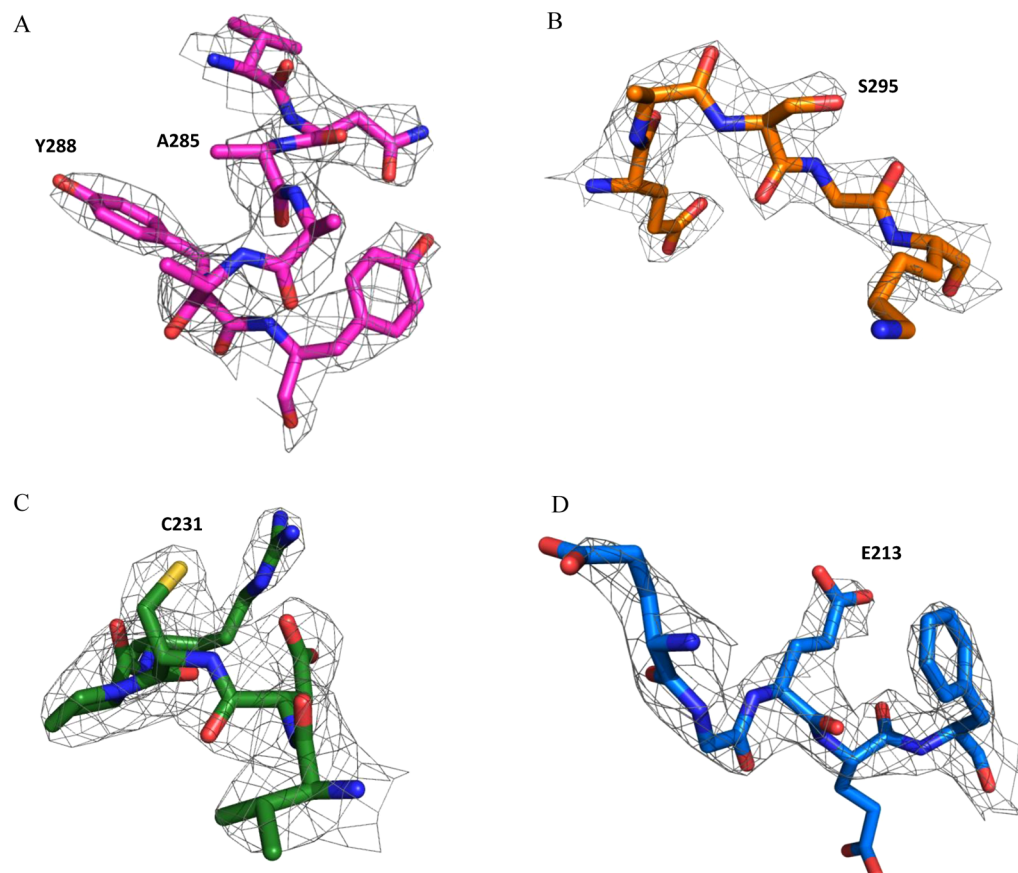


**Figure 2.**  $2mF_o - DF_c$  difference electron density map for the mutated residues contoured at  $1.5\sigma$ . (A) ASPA E285A colored magenta. (B) F295S colored orange. (C) Y231C colored green. (D) K213E colored blue. The electron density for the perturbed Tyr288 residue is also shown in the E285A structure.

large hydrophobic phenylalanine residue with a small polar serine would create a void in the core structure of this domain.

Similar to Tyr231, Glu285 is also located fairly close to the enzyme active site (Figure 3A). The  $\gamma$ -carboxyl of Glu285 forms hydrogen bonding interactions with the side chain hydroxyl of Thr118 and the backbone amide of Thr119 (Figure 3B) and is located in a loop that connects two  $\beta$ -strands in the central  $\beta$ -bundle of the native enzyme. This  $\gamma$ -carboxyl group also interacts with the backbone amide group of Ala287 in an adjacent loop. In addition, the backbone carbonyl of Glu285 is in hydrogen bonding contact with the backbone amide of Tyr288, an amino acid located within the active site cleft (Figure 3B).

**Structural Differences between the Aspartoacylase Mutants.** The overall structures of these mutant enzymes are similar to the structure of the native enzyme. Among the mutant enzymes examined in this study, the K213E mutant has the least structural perturbation, and the E285A mutant showed the greatest variances compared to the native enzyme structure. The nonconservative replacement of a positively charged amino acid with a negatively charged one would be expected to cause significant structural perturbations. However, in the case of the K213E mutation, substituting this lysine with a glutamate at position 213 does not have a substantial effect on the overall enzyme structure because there are no intraprotein interactions with this side chain  $\epsilon$ -amino group (Figure S2 of the Supporting Information). The Lys213 side chain is found to be disordered in both subunits of native ASPA, suggesting a failure to make stabilizing interactions with adjacent functional groups. In the

K213E mutant, the position of this introduced carboxyl side chain is reasonably well-defined but is still not involved in any significant interactions with other protein atoms.

The mutation at Tyr231 causes several changes in the aspartoacylase structure. The  $C\alpha$  atom of the mutated Cys231 residue moves by  $\sim 0.5 \text{ \AA}$  compared to its position in the native structure, but this introduced cysteine side chain does not participate in any new binding interactions (Figure 4). One of the adjacent amino acids, Asn284, appears to play an important structural role, as it is involved in a number of hydrogen bonding interactions with the surrounding residues. Because of the loss of balancing interactions and disruption of this hydrogen bonding network in the Y231C mutant, Asn284 is shifted slightly toward Tyr289, thereby weakening the hydrogen bond interaction of Asn284 with the backbone carbonyl oxygen of Leu187 from the other subunit. This slight movement of Asn284 causes additional structural perturbations around this residue. For example, the loop bearing the Tyr231 residue is solvent-exposed and is mainly stabilized by polar and charged residues. This loop is fairly flexible in both the native and mutant structures as indicated by the higher average temperature factors for these backbone atoms. However, in the Y231C mutant, this loop becomes even more disordered, with temperature factors for the  $C\alpha$  atoms of  $>100 \text{ \AA}^2$  in some areas of the loop. The position of this loop is stabilized in the native enzyme by the van der Waals interaction between Tyr231 and Ile239, and also by an electrostatic interaction ( $2.8 \text{ \AA}$ ) between Asp230 and Arg233. As a result of the Y231C mutation and the loss of this van der Waals contact, the Ile239 residue shifts

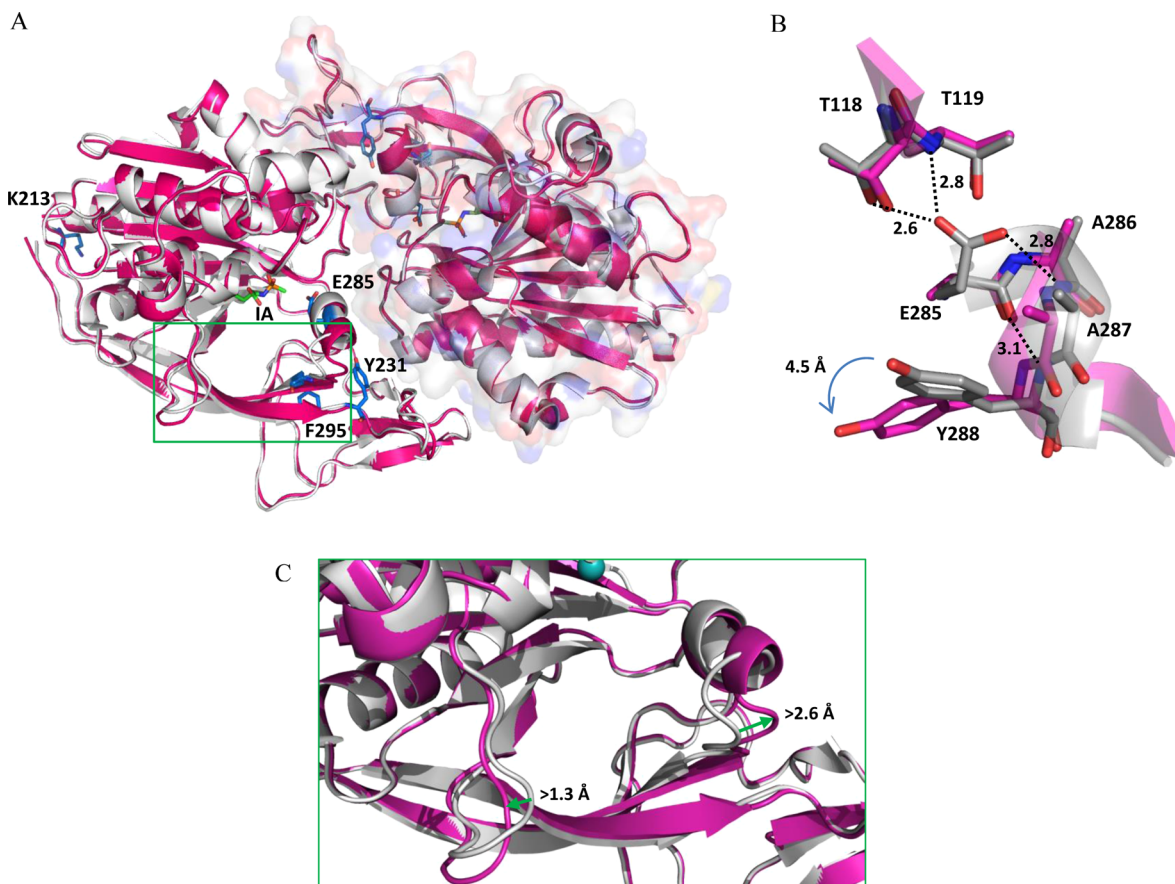


**Figure 3.** Structural comparison of aspartoacylase clinical mutant E285A with the native ASPA enzyme (PDB entry 2O4H). (A) Overall structure of ASPA E285A (magenta) superimposed with native ASPA (gray), showing the locations of the four mutation sites, and the intermediate analogue (IA) bound in the active site. (B) Participation of the Glu285 carboxylate group in a hydrogen bonding network in the native ASPA enzyme (gray) and the structural changes in ASPA E285A (magenta) resulting from the absence of these Glu285 interactions. (C) Close-up of the region near the active site showing the outward shift in the loop positions (green arrows) in the E285A structure. The zinc ion in the active site is represented as a cyan sphere.

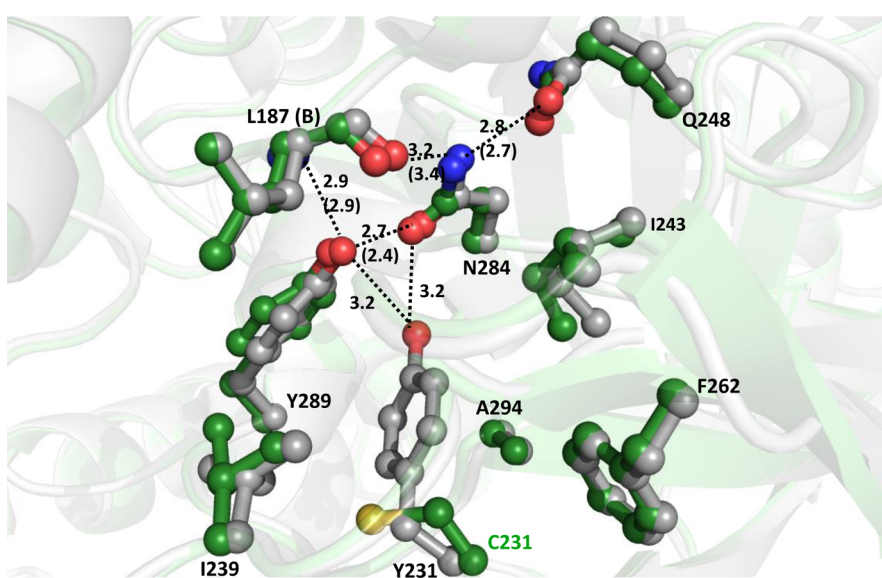


**Figure 4.** Comparison of the aspartoacylase Y231C structure with that of the native ASPA enzyme (PDB entry 2O4H). The Y231C (green) structure is superimposed with the native enzyme structure (gray) with a root-mean-square deviation of 0.33 Å for 4235 atoms. The hydrogen bond contact distances are shown for the native enzyme, with the new hydrogen bond lengths in the Y231C structure given in parentheses.

~1 Å from its original position, and the salt bridge interaction with Arg233 is subsequently weakened with the interatomic distance increasing by ~0.4 Å.

The phenylalanine to serine mutation at position 295 of ASPA causes a localized structural perturbation. Replacing this bulky phenyl group with a small polar residue creates a void in

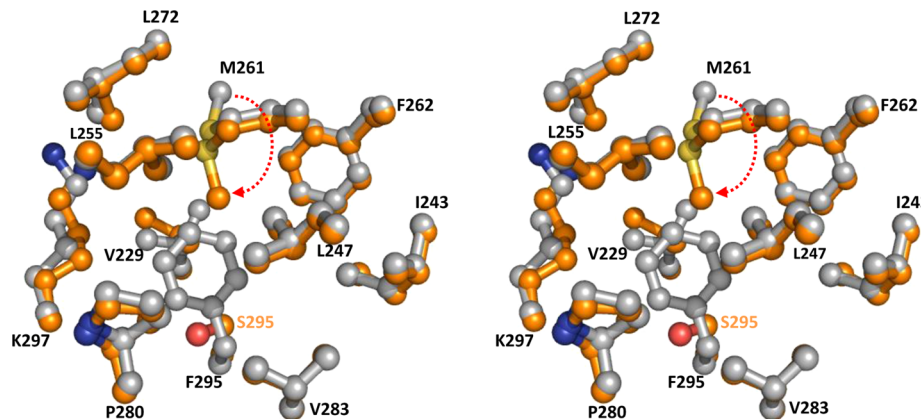


**Figure 5.** Structural comparison of aspartoacylase mutant F295S with the native enzyme (PDB entry 2O4H). Stereoview of overlaid ASPA F295S (orange) and native ASPA (gray) with a root-mean-square deviation of 0.31 Å for 4179 atoms, showing the changes in the hydrophobic core around Phe295, including the rotation of Met261 (arrow).

the core of the carboxyl domain structure that eliminates any possible stabilizing interactions with this new side chain unless these are substantial structural rearrangements in this mutated enzyme compared to the native enzyme. Instead, the side chain of Met261 moves into this void space in the F295S mutant to occupy the gap as a consequence of a change in the torsion angle around the carbon–sulfur bond, by  $\sim 160^\circ$  in subunit A (Figure 5) and  $\sim 100^\circ$  in subunit B. The side chain of Lys297 also shifts to occupy this free space through a 1 Å movement in subunit A and a 0.5 Å movement in subunit B. However, the introduced Ser295 hydroxyl side chain does not appear to make any new interactions with its surrounding environment that would help to stabilize this core structure.

Replacing the glutamate side chain at position 285 with an alanine causes substantial local structural perturbations at this site. The original position of the  $\gamma$ -carboxyl group of Glu285 is now occupied by a water molecule in the E285A structure that is hydrogen bonded (3.1 Å) to the hydroxyl of Thr118 in both subunits. The localized nature of the structural differences caused by the glutamate to alanine mutation at position 285 is best seen when the E285A mutant structure is overlaid with the native enzyme, with a root-mean-square deviation of only 0.37 Å for 4004 atoms despite this nonconservative amino acid replacement (Figure 3A). To understand how the enzyme activity of this mutant is significantly diminished, the immediate region around this mutation has been examined. The main chain and side chains of the loop formed by residues 156–166 are quite disordered, with relatively high temperature factors (Figure S3 of the Supporting Information) in the ASPA E285A binary complex structure as compared to its position in the native enzyme binary complex. This loop was also found to be disordered in native ASPA (PDB entry 2O53), but only in the apoenzyme structure,<sup>9,16</sup> suggesting a role for this structural element in response to substrate binding.

**Active Site Cavity Alterations.** The active site of ASPA is found in a deep cavity within a channel, with the substrate binding pocket composed of several lysyl and arginyl residues. These positively charged residues help to direct and orient the negatively charged NAA substrate into the active site. In the native apoenzyme, the side chains of Arg71 and Lys291 are not well-ordered, leading to an open active site channel. Upon substrate or intermediate analogue binding, conformational changes close the active site and position the substrate for catalysis. The N<sub>z</sub> atom of the Lys291 side chain now makes

a stabilizing interaction with the carboxyl oxygen of Asp68 (Figure 7), while the guanidine group of Arg71 interacts with  $\alpha$ -carboxyl group of the bound intermediate analogue in the active site of the native enzyme (Figure 6A). These new interactions are needed to orient the substrate in the active site and set up the position of the catalytic functional groups.

The structural differences that are observed in the ASPA E285A mutant are most prominent in the active site of the enzyme. The loops surrounding the active site contain two conserved amino acids, Tyr164 and Tyr288, which have moved in the E285A structure from their original C $\alpha$  positions by 1.9 Å in subunit A and by 1.3 Å in subunit B for Tyr164, and by 2.6 Å for Tyr288 (Figure 3C). These structural shifts make the active site channel much wider and more accessible even in the presence of the bound intermediate analogue.

The disruption of a stabilizing hydrogen bonding network in E285A caused by the absence of the carboxylate side chain of Glu285 leads to the displacement of the helix containing residues 285–290 and the loop containing residues 290–294. The active site residue Tyr288 in this helix is moved  $\sim 4.5$  Å from the active site in both of the enzyme subunits (Figure 3B). The phenyl oxygen of Tyr288 interacts with both the amide and the  $\alpha$ -carboxyl groups of the substrate in the native ASPA enzyme (Figure 6A). As a consequence of this altered geometry, Tyr288 is no longer able to form these hydrogen bonding interactions with the substrate in the E285A mutant (Figure 6C). The loop containing Tyr164 has also been displaced in the E285A structure, and Tyr164 has become less well ordered. Thus, the side chain hydroxyl group of Tyr164 is no longer in position to interact with the  $\beta$ -carboxyl group of the substrate (Figure 6C).

However, in the ASPA E285A structure, the active site remains open even after the intermediate analogue (and presumably the substrate) enters into the active site (Figure S6 of the Supporting Information). This failure to close the active site leaves the Arg71 side chain disordered in this mutant, along with Lys291, which is now situated in a dislocated loop. In addition, a hydrogen bond contact between the side chains of Tyr64 and Glu290, which is important to maintain active site channel architecture, is no longer present in the E285A mutant (Figure 7). In contrast, the active site channel of the other three mutants appears to function like the native enzyme, and the active site is observed to be closed in the presence of the intermediate analogue. This substrate-induced conformational change of the protein is critical

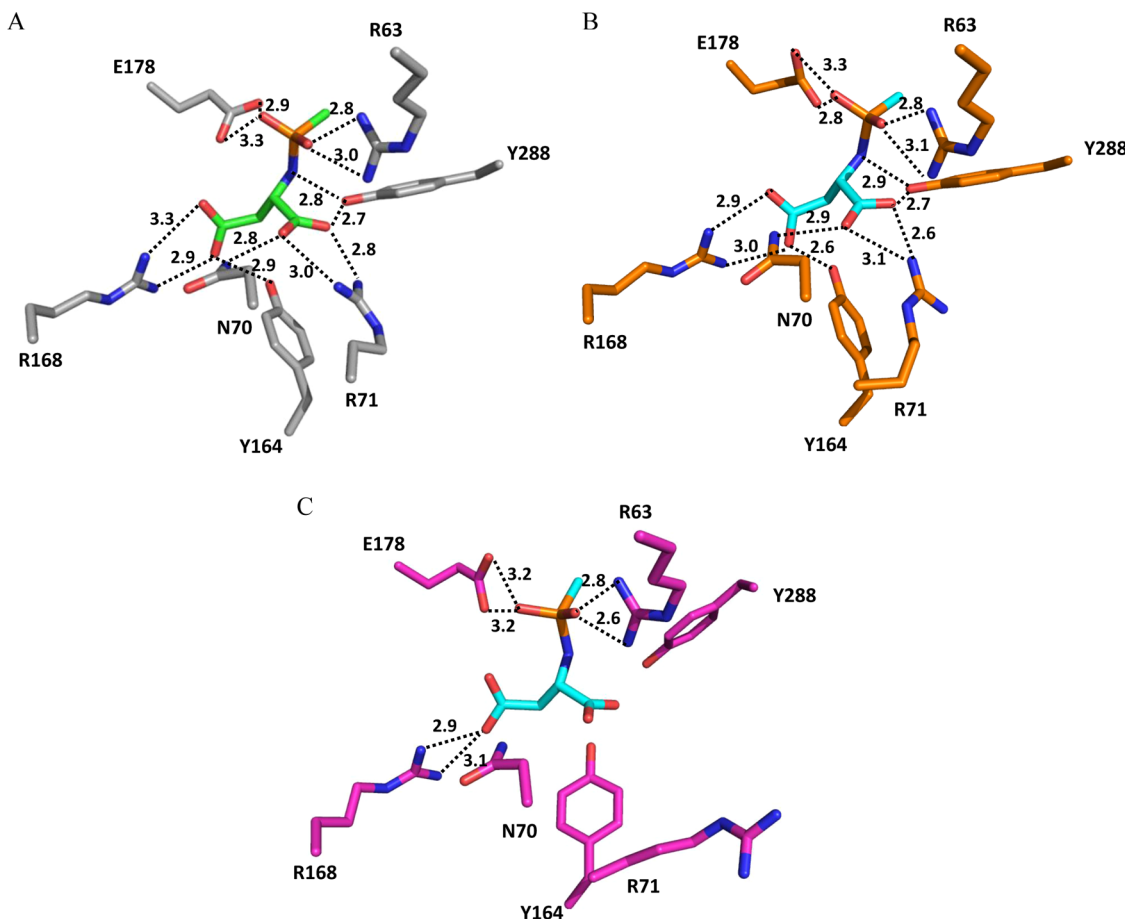


**Figure 6.** Comparison of the active site geometry of ASPA with the bound intermediate analogue *N*-phosphonomethyl-L-aspartate (green and cyan): (A) native enzyme (gray, PDB entry 2O4H), (B) ASPA F295S (orange), and (C) ASPA E285A (magenta).

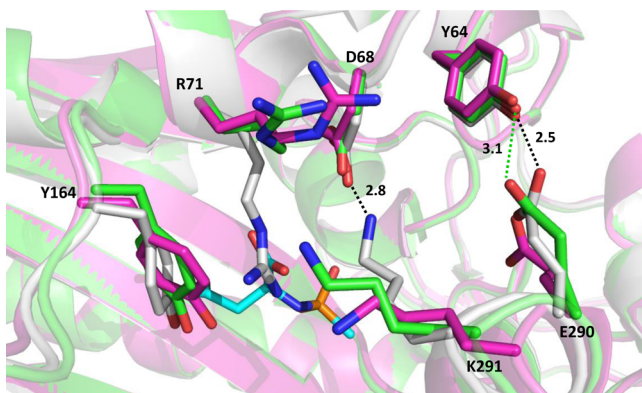


**Figure 7.** Conformational changes of Arg71 and Lys291 that occur upon binding of the intermediate analogue in the active site. Overlay of the active site cavity of ASPA, with the native apoenzyme (PDB entry 2O53) colored green, the native binary intermediate analogue complex enzyme (PDB entry 2O4H) colored gray, and the bound intermediate analogue colored blue, and the E285A binary complex enzyme colored magenta, surrounded by positively charged Arg71 and Lys291.

for the proper function of aspartoacylase and offers a likely explanation for the dramatic loss of activity in the most prevalent E285A clinical mutation.

**Structural Effects on Enzyme Catalysis.** Aspartoacylase is a metalloenzyme that belongs to the carboxypeptidase family and is active as a homodimer.<sup>16,18</sup> Each subunit of ASPA

contains one zinc ion, which acts as the catalytic center of the enzyme. The zinc ion in all four mutants (K213E, Y231C, F295S, and E285A) remains coordinated to the His21, Glu24, and His116 ligands, similar to what was observed in the native enzyme (Figure S4 of the Supporting Information). The active site Glu178 acts as the general base that activates the nucleophilic water molecule coordinated to the zinc ion and later donates a proton to assist in the departure of the L-aspartate product from the enzyme.<sup>16</sup> This catalytic residue remains intact and properly positioned in each of the mutant structures. Arg63, which stabilizes the tetrahedral intermediate formed during the reaction, is also well placed in each of these mutants to support catalysis (Figure 6). The phosphonate oxygen of the intermediate analogue that mimics the tetrahedral intermediate is coordinated to the zinc center of the mutants like in the native enzyme. Therefore, the catalytic machinery of aspartoacylase remains well-conserved and poised to conduct the catalytic reaction in these mutant enzyme forms. Nevertheless, each of these mutants has been found to be associated with the symptoms observed in Canavan disease, but leading to different clinical outcomes.

The intermediate analogue, *N*-phosphonomethyl-L-aspartate that mimics the transition state of aspartoacylase was utilized to study the mechanistic details of these mutant enzyme forms. The intermediate analogue in the native enzyme forms multiple electrostatic and hydrogen bonding interactions with multiple active site residues; among them, Asn70, Arg71, Tyr164, Arg168, and Tyr288 are important for positioning the substrate properly in the active site (Figure 6A). On the basis of the orientation of

the intermediate analogue in the active site, substrate binding in F295S (Figure 6B), Y231C, and K213E is likely the same as that observed in the native enzyme. K213E is associated with a mild disease phenotype. Any defects in the K213E mutant are not apparent from the structure, and this enzyme form has thermal stability comparable to that of the native enzyme.<sup>10</sup>

The Y231C mutation is reported to cause a mild disease phenotype, and this mutant enzyme shows fairly high catalytic activity.<sup>10,14</sup> While this mutation is found close to the active site, substrate binding is not significantly affected. Most importantly, Tyr289 can still make the same hydrogen bond interactions with the side chain carbonyl of Asn284 and the backbone carbonyl of Leu187 from the adjacent subunit that serves to orient Tyr288 in the active site. However, structural anomalies that arise from the Y231C mutation result in compromised thermal stability.<sup>10</sup> In addition, because Tyr231 is present at the origin of a coil structure in the carboxyl-terminal domain, this tyrosine appears to make critical interactions with the surrounding residues that may facilitate proper folding of the carboxyl domain around the rest of the protein structure to form a functional enzyme.

The diminished activity of the F295S mutant most likely results from the decreased stability of the protein<sup>10</sup> as a consequence of the perturbations in the core of the carboxyl domain structure. Immunoblotting studies of the ASPA enzyme expressed in COS-7 cells have shown that the F295S mutant yields very low protein levels despite the similar level of mRNA compared to that of the native enzyme.<sup>17</sup> In the same study, the K213E and E285A mutants were found to express similar amounts of enzyme compared to that of native ASPA. Among these four mutations, the F295S and Y231C mutations yield somewhat reduced levels of protein in the *P. pastoris* expression system employed in our laboratory (data not shown). Therefore, the Y231C and F295S mutants both appear to suffer from protein stability and folding issues that would likely limit their lifetimes in the brain of CD patients.

ASPA E285A is one of the lowest-activity mutants examined, and this enzyme form also has very low thermal stability compared to that of the native enzyme.<sup>10</sup> In addition, the substrate binding residues in the active site of this mutant are not correctly positioned to interact with and orient the substrate (Figure 6C). The Tyr288 that forms a hydrogen bond interaction with the  $\alpha$ -carboxyl and the amide nitrogen of the intermediate analogue has moved away from the active site. The Arg71 and Tyr164 side chains are each not well ordered in the E285A mutant structure (Figure S5 of the Supporting Information). Tyr164 does appear to be capable of making a hydrogen bond contact with the  $\alpha$ -carboxyl of the substrate in one of the monomers in the structure. Similarly, in one of the monomers, Asn70 and Arg168 are positioned to form stabilizing interactions with the  $\beta$ -carboxyl group of the intermediate analogue. Thus, the orientation of the substrate in each monomer of the E285A mutant has been altered. The loss of activity in ASPA E285A is a direct result of the distorted architecture in the active site. These differences in binding of the substrate to the active site of the E285A mutant are also supported by the 5-fold higher  $K_i$  value observed for the intermediate analogue for this mutant ( $1.48 \pm 0.13 \mu\text{M}$ ) compared to that for the native enzyme ( $0.33 \pm 0.05 \mu\text{M}$ ). In addition, *N*-acetyl-L-glutamate, a homologue of NAA with one additional carbon, was found to selectively interact with the E285A mutant. This mutant enzyme is inhibited by *N*-acetyl-L-glutamate (NAG) with a  $K_i$  of  $0.84 \pm 0.08 \text{ mM}$ , whereas this compound does not show any measurable inhibition of the

native enzyme when examined at concentrations of up to 5 mM. The inhibition of E285A by NAG can be overcome by increasing the concentration of NAA, confirming its competitive inhibition versus the substrate. This selective binding of NAG to the active site cavity of ASPA E285A is a direct consequence of the altered active site structure of this mutant. Introduction of a conserved mutation at this position (E285D) has been found to produce an enzyme form with activity and stability that are both significantly higher than those of the E285A mutant.<sup>11</sup> We can conclude that the negatively charged glutamate residue at position 285 is clearly essential for maintaining the aspartoacylase structure and supporting its catalytic function even though this side chain functional group does not directly participate in substrate binding or catalysis.

## CONCLUSIONS

Mutations throughout the ASPA gene lead to aspartoacylase enzyme forms with impaired catalytic efficiency. The non-conservative replacement of Lys213 with glutamate has minimal catalytic and structural consequences because of the surface location and lack of intraprotein interactions. Replacement of bulky Tyr231 and Phe295 in the hydrophobic core of the enzyme results in decreased protein stability. The negatively charged glutamate residue at position 285 is clearly essential for maintaining the aspartoacylase structure and supporting its catalytic function even though this side chain functional group does not directly participate in substrate binding or catalysis. These novel structural insights into the ASPA catalytic deficiencies will provide the basis for the design of small molecule compounds to bind and potentially stabilize the lower-stability aspartoacylase clinical mutants. Such compounds would serve as pharmacological chaperones for the treatment of Canavan disease.

## ASSOCIATED CONTENT

### S Supporting Information

Oligomeric states of the aspartoacylase clinical mutants in solution, as determined by dynamic light scattering and native gel electrophoresis, and additional structural information for ASPA clinical mutations, including the catalytic centers of the mutant enzymes and the  $2\text{mF}_\text{o}-\text{DF}_\text{c}$  electron densities at the active sites of both subunits of the E285A mutant. This material is available free of charge via the Internet at <http://pubs.acs.org>.

### Accession Codes

The atomic coordinates and structure factors have been deposited in the Protein Data Bank as entries 4MRI (ASPA F295S), 4MXU (ASPA K213E), 4TNU (ASPA Y231C), and 4NFR (ASPA E285A).

## AUTHOR INFORMATION

### Corresponding Author

\*E-mail: ron.viola@utoledo.edu. Telephone: (419) 530-1582. Fax: (419) 530-1583.

### Funding

This work was partially supported by grants from the Canavan Research Foundation and the Jacob's Cure Foundation.

### Notes

The authors declare no competing financial interest.

## ACKNOWLEDGMENTS

We thank GM/CA CAT at the Advanced Photon Source, Argonne National Laboratory. We also thank Dr. Amarjit Luniwal (The University of Toledo) for synthesis of the intermediate analogue *N*-phosphonomethyl-L-aspartate.

**■ REFERENCES**

- (1) Kumar, S., Mattan, N. S., and de Vellis, J. (2006) Canavan disease: A white matter disorder. *Mental Retardation and Developmental Disabilities Research Reviews* 12, 157–165.
- (2) Traeger, E. C., and Rapin, I. (1998) The clinical course of Canavan disease. *Pediatric Neurology* 18, 207–212.
- (3) Kaul, R., Gao, G. P., Aloya, M., Balamurugan, K., Petrosky, A., Michals, K., and Matalon, R. (1994) Canavan disease: Mutations among Jewish and non-Jewish patients. *Am. J. Hum. Genet.* 55, 34–41.
- (4) Matalon, R., Kaul, R., Casanova, J., Michals, K., Johnson, A., Rapin, I., Gashkoff, P., and Deanching, M. (1989) SSIEM Award. Aspartoacylase deficiency: The enzyme defect in Canavan disease. *J. Inherited Metab. Dis.* 12 (Suppl. 2), 329–331.
- (5) Matalon, R., and Michals-Matalon, K. (1999) Biochemistry and molecular biology of Canavan disease. *Neurochem. Res.* 24, 507–513.
- (6) Chakraborty, G., Mekala, P., Yahya, D., Wu, G., and Ledeen, R. W. (2001) Intraneuronal N-acetylaspartate supplies acetyl groups for myelin lipid synthesis: Evidence for myelin-associated aspartoacylase. *J. Neurochem.* 78, 736–745.
- (7) Surendran, S., Matalon, K. M., Tyring, S. K., and Matalon, R. (2003) Molecular basis of Canavan's disease: From human to mouse. *Journal of Child Neurology* 18, 604–610.
- (8) Madhavarao, C. N., Arun, P., Moffett, J. R., Szucs, S., Surendran, S., Matalon, R., Garbern, J., Hristova, D., Johnson, A., Jiang, W., and Namboodiri, M. A. (2005) Defective N-acetylaspartate catabolism reduces brain acetate levels and myelin lipid synthesis in Canavan's disease. *Proc. Natl. Acad. Sci. U.S.A.* 102, 5221–5226.
- (9) Bitto, E., Bingman, C. A., Wesenberg, G. E., McCoy, J. G., and Phillips, G. N., Jr. (2007) Structure of aspartoacylase, the brain enzyme impaired in Canavan disease. *Proc. Natl. Acad. Sci. U.S.A.* 104, 456–461.
- (10) Zano, S., Wijayasinghe, Y. S., Malik, R., Smith, J., and Viola, R. E. (2013) Relationship between enzyme properties and disease progression in Canavan disease. *J. Inherited Metab. Dis.* 36, 1–6.
- (11) Moore, R. A., Le Coq, J., Faehnle, C. R., and Viola, R. E. (2003) Purification and preliminary characterization of brain aspartoacylase. *Arch. Biochem. Biophys.* 413, 1–8.
- (12) Tacke, U., Olbrich, H., Sass, J. O., Fekete, A., Horvath, J., Ziyyeh, S., Kleijer, W. J., Rolland, M. O., Fisher, S., Payne, S., Vargiami, E., Zafeirou, D. I., and Omran, H. (2005) Possible genotype-phenotype correlations in children with mild clinical course of Canavan disease. *Neuropediatrics* 36, 252–255.
- (13) Shaag, A., Anikster, Y., Christensen, E., Glustein, J. Z., Fois, A., Michelakis, H., Nigro, F., Pronicka, E., Ribes, A., Zabot, M. T., et al. (1995) The molecular basis of canavan (aspartoacylase deficiency) disease in European non-Jewish patients. *Am. J. Hum. Genet.* 57, 572–580.
- (14) Rady, P. L., Vargas, T., Tyring, S. K., Matalon, R., and Langenbeck, U. (1999) Novel missense mutation (Y231C) in a turkish patient with canavan disease. *Am. J. Med. Genet.* 87, 273–275.
- (15) Kaul, R., Gao, G. P., Balamurugan, K., and Matalon, R. (1993) Cloning of the human aspartoacylase cDNA and a common missense mutation in Canavan disease. *Nat. Genet.* 5, 118–123.
- (16) Le Coq, J., Pavlovsky, A., Malik, R., Sanishvili, R., Xu, C., and Viola, R. E. (2008) Examination of the mechanism of human brain aspartoacylase through the binding of an intermediate analogue. *Biochemistry* 47, 3484–3492.
- (17) Hershfield, J. R., Pattabiraman, N., Madhavarao, C. N., and Namboodiri, M. A. (2007) Mutational analysis of aspartoacylase: Implications for Canavan disease. *Brain Res.* 1148, 1–14.
- (18) Le Coq, J., An, H. J., Lebrilla, C., and Viola, R. E. (2006) Characterization of human aspartoacylase: The brain enzyme responsible for Canavan disease. *Biochemistry* 45, 5878–5884.
- (19) Otwinowski, Z., and Minor, W. (1997) Processing of X-ray Diffraction Data Collected in Oscillation Mode. *Methods Enzymol.* 276, 307–326.
- (20) Murshudov, G. N., Vagin, A. A., and Dodson, E. J. (1997) Refinement of macromolecular structures by the maximum-likelihood method. *Acta Crystallogr. D53*, 240–255.
- (21) Emsley, P., and Cowtan, K. (2004) Coot: Model-building tools for molecular graphics. *Acta Crystallogr. D60*, 2126–2132.
- (22) DeLano, W. L. (2002) *The PyMOL Molecular Graphics System*, DeLano Scientific, San Carlos, CA.